Mater. Res. Soc. Symp. Proc. Vol. 845 © 2005 Materials Research Society AA1.9

Simulations of Chemotaxis and Random Motility in Finite Domains

Ehsan Jabbarzadeh and Cameron F. Abrams
Department of Chemical Engineering
Drexel University
3141 Chestnut St.
Philadelphia, PA 19104

ABSTRACT

Rational design and selection of candidate porous biomaterials to serve as tissue engineering constructs rests on our ability to understand the influence of the porous microarchitecture on the transport of chemical species (e.g., nutrients and signaling compounds), fluid flow, and cellular locomotion and growth. We have begun to study the behavior of chemotactically mobile cells in response to unsteady signaling molecule concentration fields using a computational simulation-based model. The model couples fully time-dependent finite-difference solution of a reaction-diffusion equation for the concentration field of a generic chemoattractant to biased random walks representing individual moving cells. This model is a first step in building a quantitative, pore-level model of mass and cellular transport in porous tissue-engineered constructs. In these proceedings, we focus on our recent findings regarding the influence of flux-reactive boundary conditions in heterogeneous 2D domains on the chemotactic response of otherwise randomly moving cells. In particular, we find that, when cells are forced to "crawl" around obstacles in order to approach a point source of chemoattractant, the reactivity of the obstacle surface with respect to the chemoattractant strongly determines the morphology of the cells' paths of locomotion. Cells crawl along non-reactive surfaces and strongly avoid reactive surfaces, due to the nature of the chemoattractant concentration gradients near the surface. We show further that tuning the reactivity of the surfaces of two obstacles defining a gap can control the passage of cells through the gap. From our work, we infer the importance of a proper treatment of boundary conditions in any future pore-level quantitatve modeling of mass transport and cellular response in porous media.

INTRODUCTION

Current technology gives us the ability to construct a wide variety of porous biomaterials for therapeutic applications, including tissue engineering and immuno-isolated implants. In fact, this ability far outpaces our understanding, at a fundamental level, of why one porous material performs better than another in any given application. In many applications, one of the most important performance requirements is that the material allow for easy development of healthy, internal capillary networks [1]. This neovascularization within an implant greatly reduces the impediment to biochemical transport relative to diffusion through the otherwise present fibrous capsule characteristic of the classical foreign body response (FBR) [2]. Mitigating the FBR in this way allows for optimal nutrient/waste transport for engineered tissues grown on porous scaffolds [3] and has the potential to guarantee rapid, controllable dosing in drug delivery and

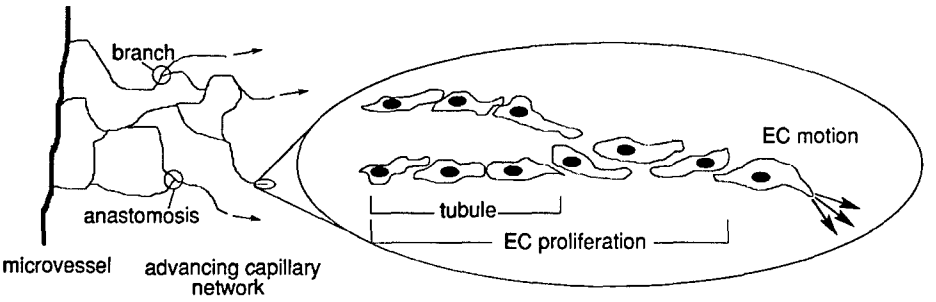

Figure 1. Schematic of capillary sprout growth in angiogenesis, showing a close-up of the tip in longitudinal cross-section.

immuno-isolated gene and cell-based implant therapies [4]. It is therefore vitally important that we explore ways to control this neovasculature development. One goal must be incorporating this ability, which we refer to as "directed angiogenesis," into design strategies for porous biomaterials. This requires in part a fundamental understanding of the interactions between porous microstructures and growing capillary sprouts.

The directed migration of endothelial cells (ECs) is the mechanism underlying the construction of capillary networks as a response to stimulants such as vascular endothelial growth factor (VEGF) and tumor angiogenic growth factor (TAF) [5]. The morphology of a sprout is determined by (i) the biased locomotion path of the single EC at the sprout tip, and (ii) the proliferation of cells in the tubule following the sprout tip, as depicted in figure 1. The EC locomotion is directed over large length scales, while at small length scales it is apparently random, owing to inhomogeneities in the ECM and void space through which these cells must crawl, as well as concentration variations in stimulants and nutrients, among others. This biased locomotion is categorized as a mixture of "chemotaxis," in which the direction of cell motion is influenced by external concentration gradients, and "chemokinesis," in which the speed of cell motion is influenced by these gradients.

There is evidence in the experimental literature that chemotaxis can be harnessed to induce EC penetration of porous scaffolds which would normally not allow for EC penetration. Various biocompatible porous scaffold materials, including expanded poly(tetrafluoroethylene) (ePTFE) [6] and poly(vinyl alcohol) [3], have been shown to admit EC penetration in vitro when the mean pore size is greater than $\sim$60 μm. However, Kidd et al. showed that when an ePTFE disc is treated with cellular detritus rich in growth factors on one side, microvessel penetration is possible even through pores as small as 30 μm [7]. A similar pretreatment strategy was employed by Sanders et al., who demonstrated the feasibility of "prevascularizing" a polyurethane mesh biomaterial implant by placing it in temporary contact with the relatively active vasculature of the chorioallontoic membrane of quail embryos [8]. The quail vasculature readily penetrated the implant, which was subsequently removed from contact with the membrane and implanted

in rats. This means that both sets of authors inferred that concentration gradients of some type of signaling molecule influenced the direction and location of vessel growth.

The great interest in the biomaterials community in directed angiogenesis has led to a variety of empirical optimization approaches. The biomaterials engineer can imagine and construct a variety of materials with different microporous architectures, can biochemically modify these structures, and design any number of protocols for *ex vivo* culturing. In the face of this variety, we must place rational limits on the amount of trial-and-error, and therefore the expense, required to decide which porous biomaterial design strategy best suits a particular application. A significant step forward in this regard would be a simulation model which allows for rapid in virtuo testing of a proposed microarchitecture, together with a proposed biochemical pretreatment and culturing protocol, prior to its fabrication and in vitro/in vivo testing. Such a model must, at a minimum, capture the 3-D microstructure of a porous material and account for chemotaxis and chemokinesis in cell migration, to quantify effects of length scales and correlations in the porous structure and biochemical pretreatment techniques on the rate of cell penetration.

No such model yet exists. However, our work toward such a model has led us to investigate chemotactic locomotion in well-controlled simulations in inhomogeneous 2D domains. Living cells are too complicated to model with complete accuracy. In multicellular simulations, simple rules governing cell behavior are imposed, and emergent behavior from cell populations is observed and analyzed. A "cell" is a computational entity that can move, divide, die, perhaps transform itself, consume nutrients, and produce wastes. The task of the simulation developer is to come up with sensible rules governing this behavior, so that, to an observer, the cell mimics the behavior of a living cell. This non-trivial task means that several dozen parameter values must be carefully assigned based on existing experimental results, and in some instances, free parameters are fit to experimental results in the process of building the model.

A popular method in multicellular simulations is cellular automata (CA). In CA, an automaton is an array of "cells" (not in the biological sense), each being a box in space that can have one of many states. In biological applications, a cell can be unoccupied, or occupied with a computational cell. In each simulation pass or time-step, each occupied cell is given the chance to change its state based on its local environment. Relatively simple rules for division and death result in surprisingly rich and structured behaviors, as anyone who has watched J. H. Conway's "Game of Life" screensaver can attest [9]. A relatively more complex set of rules was used to model growing endothelial cells in pioneering work by Zygourakis et al. (e.g., [10, 11]). Quite recent work has used CA in conjunction with simple transport models to probe the effects cell-to-cell signaling in the development of microvascular structures [12].

A related technique in multicellular simulations is the biased random walk (BRW) [13, 14, 15]. This type of model has found widespread use in the simulation of angiogenesis. This path may generally tend toward a source of chemoattractant, but also has some tunable random contribution. Most studies to date have assumed that the concentration field of chemoattractant is steady in time. The only true distinction between CA and BRW cell models is that CA restricts cell positions to lattice sites, which BRW are typically off-lattice. In only one instance has a BRW multicellular simulation been coupled with the fully transient solution of a reaction-diffusion equation for chemoattractant [14],

and this was done in a 2D homogeneous domain. This is a significant advance because it dynamically coupled the concentration of chemoattractant and migrating cells. Tong and Yuan [14] demonstrated that this interplay is responsible for the well-known "brush-border" effect. in which a very high density of capillary branching occurs near the source of a growth factor, screening the parent vessel from the growth factor and ultimately slowing the total process of angiogenesis.

We have developed a BRW multicellular simulation in the same spirit of Tong and Yuan, with an eye toward the eventual development of a multicelluar/transport simulation model of tissue ingrowth in porous constructs. The purpose of this contribution is to discuss our recent work investigating the effect of surfaces which consume chemoattractant on the chemotactic response of crawling cells in heterogeneous 2D domains. The goal generally is to understand how both the geometry and reactivity of surfaces in a structured domain modulate concentration fields of stimulants (chemoattractants) and how these modulations can be engineered to control cell locomotion.

MODEL AND SIMULATIONS

Our model, described in detail elsewhere [16], includes (1) a fully time-resolved finite difference solution which governs the transport of chemoattractant, and (2) a "biased" random walk simulation of mobile cells which couples the direction of cell motion to the simultaneously evolving concentration field of chemoattractant. The model considers the following fundamental events: (i) release of a chemoattractant from sources or cells; (ii) diffusion of chemoattractant in the domain; (iii) randomness in the direction of cell migration, presumably due to other underlying variables which yet we do not have enough information; (iv) chemotactic response of cells.

Transport of chemoattractant

The major task of the finite difference solver is to obtain the concentration of chemoattractant as a function of position and time, $c(\mathbf{r}, t)$ (boldface denotes a vector quantity). The governing transport equation is as follows:

$$\frac{\partial c}{\partial t} = \mathcal{D}\nabla^2 c + \sum_i \frac{P_i(t)}{v_c}\delta(\mathbf{r} - \mathbf{r}_i), \tag{1}$$

where $\mathcal{D}$ is the diffusivity of chemoattractant and $\mathbf{r}_i$ is the location of the i'th point source. Point sources produce at a rate $P(t)$. v_c is the volume of a cell, so $\frac{P_i(t)}{v_c}$ represents the rate at which the concentration of chemoattractant is introduced by a point source at position $\mathbf{r}_i$. $\delta(x)$ is the Dirac delta function:

$$\delta(x) = \begin{cases} 1, & x = 0 \\ 0, & x \neq 0 \end{cases} \tag{2}$$

For simplicity at this stage of model development, cell division, uptake and degradation of chemical species are neglected. Numerical values of the relative quantities in this model appear in Table I. Eq. 1 is solved numerically using a finite-difference technique referred to

as the "hopscotch method" [17, 18]. The 2D homogeneous solution domain measures 2 mm × 2 mm, as shown in Fig. 2, and is discretized onto a mesh of 200×200 nodes. The origin of the domain is the lower-left corner, and the center point of the domain is node (100,100). From here on, lengths are reported in units of mm unless otherwise stated.

The following initial and boundary conditions on the solution $c(\mathbf{r}, t)$ are enforced:

$$c(\mathbf{r}, 0) = 0 \tag{3}$$

$$-\mathcal{D}\nabla c = kc \tag{4}$$

Eq. 4 represents reactive boundary conditions applied along boundary curves in the domain. The proportionality constant k measures the reactivity of the boundaries. For this early stage study, we have assumed first order kinetics. As is standard in these types of "reaction-diffusion" problems, the dimensions of the constant k are length/time; we choose to measure k in units of cm/s. The various boundary curve geometries considered (defining the heterogeneous domains) is described in the "**Simulation Protocols**" section.

The dimensionless parameter which measures whether diffusion or reaction dominates the boundary condition given in Eq. 4 is the Péclet number:

$$\mathrm{Pe} = \frac{kh}{\mathcal{D}}, \tag{5}$$

where we have chosen the lattice spacing h as the relavent length scale. For the parameters given in table I ($\mathcal{D} = 10^{-6}$ cm^2/s, $h = 10^{-3}$ cm), in addition to considering the case of $k = 0$ (i.e., "no-flux" boundaries), we have chosen to sweep values of k from a "low" Pe of 10^{-3} to a "high" Pe of 100.

As presented, the only sink for chemoattractant so far discussed is reaction at boundary curves, controlled by the reactivity k. Additionally, we employ "global" boundary conditions of Dirichlet type; these too are discussed in the "**Simulation Protocols**" section.

Biased random walk simulation of chemotaxis

Random walks are propagated in the following way. We first stipulate that a walker make a step *on average* with a frequency f_T, and that step lengths are randomly chosen from a Gaussian distribution with mean $\langle \Delta l \rangle$ and standard deviation $\sigma_{\Delta l}$. f_T and $\langle \Delta l \rangle$ are constrained relative to one another to guarantee that, over long times, cells move with an average velocity, v_0, observed experimentally. We freely choose f_T and $\sigma_{\Delta l}$, but these values (shown in table I) are the same for all simulations discussed here. For each mesh update (every 2 s of integration time) each cell in the simulation is given the opportunity to move. The probability that a cell will take a step is the probability of observing an event which occurs with a frequency f_T in a time interval Δt: $P_T = f_T \Delta t$. If a uniform random variate between 0 and 1 is chosen less than P_T, the cell under consideration takes a step. The direction of a step, denoted by the unit vector $\hat{\mathbf{p}}$, is computed as

$$\mathbf{p} = \alpha \frac{\mathbf{r}(t) - \mathbf{r}(t - \Delta t_{\mathrm{cell}})}{|\, \mathbf{r}(t) - \mathbf{r}(t - \Delta t_{\mathrm{cell}}) \,|} + \beta \frac{\nabla c}{|\, \nabla c \,|} + (1 - \alpha - \beta)\boldsymbol{\lambda}. \tag{6}$$

Table I. Nomenclature: Baseline values or ranges of important model parameters.

Parameter	Description	Value or Range
Δt_{conc}	Time step for mesh update	2 s
h	Mesh discretization	10 μm
$\mathcal{D}$	Growth factor diffusivity	10^{-6} cm^2/s [14]
P	Chemoattractant production rate per cell	1 pg/h [19]
f_T	Average frequency of random walk updates	0.0167 s^{-1}
v_{max}	Maximum cell speed	20 μm/h [13]
$\langle \Delta l \rangle$	Mean step length	0.333 μm
$\sigma_{\Delta l}$	Width of Gaussian step length distn.	0.083 μm
α	Step persistence parameter	0
β	Step chemotactic parameter	0-1
r_c	Cell radius	10 μm [14]
v_c	Cell volume	$\approx \frac{4}{3}\pi r_c^3$
k	Rate constant for boundary reactivity	0 and 10^{-6}-0.1 cm/s

The vector $\mathbf{p}$ is the weighted sum of three unit vectors. The first term, which is weighted by α, defines persistence, representing the fact that mobile cells keep a "memory" of their previous step direction. The second term, which is weighted by β, represents the chemotactic response. The final term, carrying the remainder of the weight, is a random direction, $\boldsymbol{\lambda}$, chosen uniformly. We interpret this "random" component of the direction as a lumping together of all underlying processes governing cell migration for which we have no information or purposely ignore for simplicity. Also for reasons of simplicity in this early study, we have chosen to neglect persistence, setting α to 0 for all cases.

The motion of cells are coupled to the transport of chemoattractant because a cell must "measure" a local concentration gradient. Because cell positions are off-lattice, a cell at an arbitrary location in 2D space samples c and ∇c by linear interpolation among the four nodes nearest it. At each cell position update, the instant values of average c and ∇c are used in the determination of $\mathbf{p}$. When a cell injects chemoattractant into the domain, it likewise partitions the amount over the four nodes nearest it via linear interpolation.

An important component of the model is the pair of threshold conditions required for chemotactic response. In optimal conditions, cells can detect a 1 percent difference in concentration of chemoattractant along their length [20]. It has also been shown in experiments that high chemoattractant concentration results in cell movements which are completely decorrelated from the direction of a chemoattractant gradient [21]. Therefore, we prescribe that the coefficient β also serve as a switch on the chemotactic response. For any particular cell's average c and ∇c, the value of β used to determine the direction of its next step is set to 0 if ${}^{\nabla c}_{c} r_c < 0.005$, which we refer to as the "gradient threshold." We also employ a "concentration threshold," setting $\beta = 0$ when $c < 10^{-10}$ g/cm^3 [19].

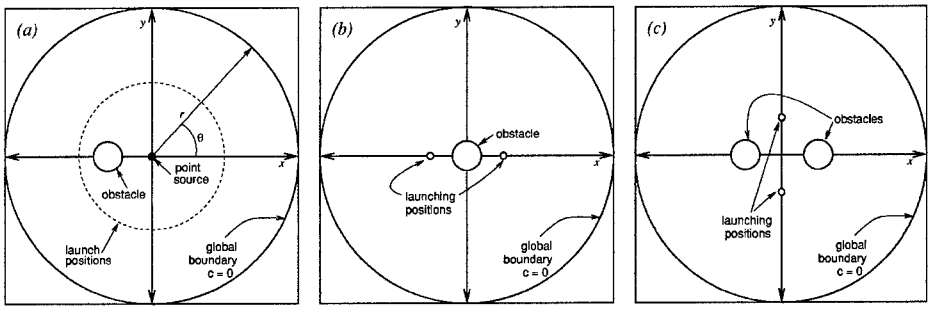

Figure 2. Schematic simulation domains for the four types of chemotaxis simulations considered here. (a) Single walkers around single obstacle. (b) Dual walkers around single obstacles. (c) Dual walkers around dual obstacles.

Simulation Protocols

Single walks around single obstacles

We first consider the simple scenario in which an immobile point source at the center point produces chemoattractant at a constant rate ($P = 1$ pg/h). Cells are launched from a distance of 0.5 mm from the source for randomly chosen values of polar angle, θ. A circular "obstacle" of diameter 0.2 mm is located 0.3 mm to the left of the source (figure 2a). A global Dirichlet-type boundary condition, $c(R,t) = 0$, is enforced at $R =$ 1 mm. 100,000 walks are conducted for various values of chemotacticity β and surface reactivity k. The primary observable is the time required for the cells to traverse the 0.5 mm distance from the launching radius to the source, referred to as the "time-to-contact," t_c, as a function of angular position, θ.

Dual walks around single obstacles

We next consider the scenario in which two cells are placed initially 0.4 mm apart with the midpoint of the segment defined by their positions lies on the center point. Centered on the center point is a circular obstacle of diameter 0.2 mm (figure 2b). The same global Dirichlet boundary condition from the previous case is employed. The two cells produce chemoattractant in pulses defined by a duty cycle: secretion at a rate of $6P$ for a random "on" time, t_{on}, selected uniformly in the range 10 min $< t_{\text{on}} <$ 30 min, followed by no secretion for a random "off" time, t_{off}, selected uniformly in the range 50 min $< t_{\text{off}} <$ 150 min. (We demonstrated previously that this random "pulsed" secretion of chemoattractant guarantees that two cells can successfully signal one another in a homogeneous domain [16].) 100 statistically equivalent individual dual-cell simulations are performed for various values of β and k. The primary observable is the time required for

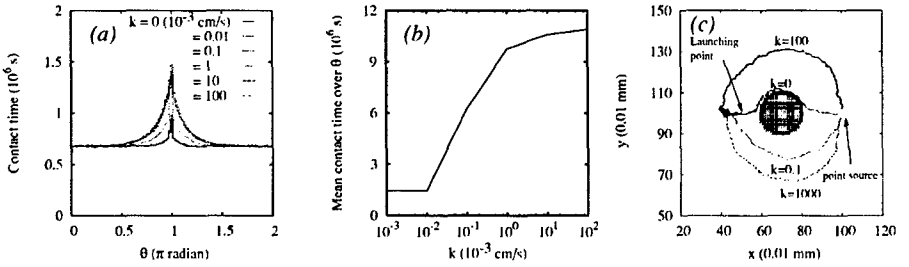

Figure 3. (a) Distributions in time-to-contact over θ, for single walkers in the domain with the single obstacle, for various obstacle boundary reactivities k; units of k in the figure are 10^{-3} cm/s. (b) Mean of each distribution in (a). (c) Example locomotion paths for selected reactivities; $\beta = 0.30$.

the two cells to reach one another, again referred to as the "time-to-contact," t_c.

Dual walks around dual obstacles

The next scenario we consider is similar to the previous, except that we now place two circular obstacles of diameter 0.2 mm separated by a distance D, with their midpoint on the center point. The quantity $L = D$ - 0.2 mm is referred to as the "gap spacing," as this is the minimal distance between the two bounding curves of the obstacles. Dual cells are launched at 180° opposition such that, in order to reach one another, they must crawl through the gap between the obstacles (figure 2c). We examined the effects of both surface reactivity k and gap spacing L on the chemotactic signaling and response of the two cells. Here, the primary observable is whether particular values of k and L permit successful passage by one or both cells. Our aim is to make a first attempt at understanding the synergistic roles of both pore size and surface reactivity on chemotactic response in a simple model system.

RESULTS AND DISCUSSION

Single walks around single obstacles

In figure 3a, we present the time-to-contact distributions as a function of angle θ for the case of a single obstacle offset from the origin. Each curve represents the results of runs with different obstacle boundary reactivity, k. First, note the expected result that, in general, for cells launched in the vicinity of $\theta = \pi$, for which the point source at the origin is eclipsed by the obstacle, the contact time is higher than the average. We see that, the more reactive the surface, the more influence is felt by the contact time distribution. We show the mean of each distribution in figure 3b. The contact time appears most sensitive to k in the range 10^{-5} cm/s $< k < 10^{-3}$ cm/s. The saturation at high reactivities is

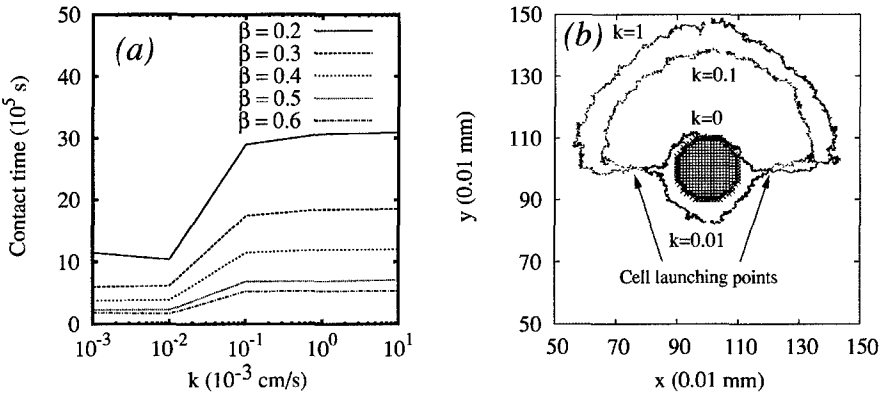

Figure 4. (a) Mean contact time for two cells forced to move around an obstacle vs. obstacle boundary reactivity, k, to secreted chemoattractant, for various chemotacticities, β. (b) Example locomotion paths from the dual-cell, single-obstacle runs, for various obstacle boundary reactivities; $\beta = 0.30$.; values of k in the figure are in units of 10^{-3} cm/s

unambiguously determined by the global boundary condition at $r = R$. As can be seen in figure 3c, for highly reactive surfaces, cells initially move *away* from both the obstacle and the point source. This is because ∇c always points away from reactive boundaries. Because of the global boundary, there must exist a radius at which ∇c in the r direction in the vicinity of $\theta = \pi$ changes sign. In this region, the gradient threshhold is violated and cells "lose signal" for some time until they can diffuse into a region in which some gradients are detectable. These gradients invariably lead the walkers around the obstacle to the source. We learn from this small study that, because reactive surfaces cause gradients in c which point away from the surface, chemotactically active cells tend to avoid reactive surfaces, even if that leads them further from a point source of chemoattractant.

Dual walks around single obstacles

In figure 4a, we show the mean contact times for two chemotactically active mobile cells, each producing chemoattractant using the pulsed protocol described previously, vs. obstacle boundary reactivity for various values of chemotacticity. For each k and β, 100 individual simulations contribute to each average. We observe a similar trend as that seen for the single walkers, namely, that the greatest sensitivity to k occurs in the range 10^{-5} cm/s $< k < 10^{-3}$ cm/s. Furthermore, the stronger the chemotacticity, the smaller is the influence of the boundary reactivity on the mean contact time. We also show example locomotion paths in figure 4. This illustrates the reason for this sensitivity: for large reactivities, cells initially move away from the obstacle and each other, until feeling the influence of the global boundary, at which time they are led to one another while "confined" between the obstacle at the origin and the global boundary. The stronger the

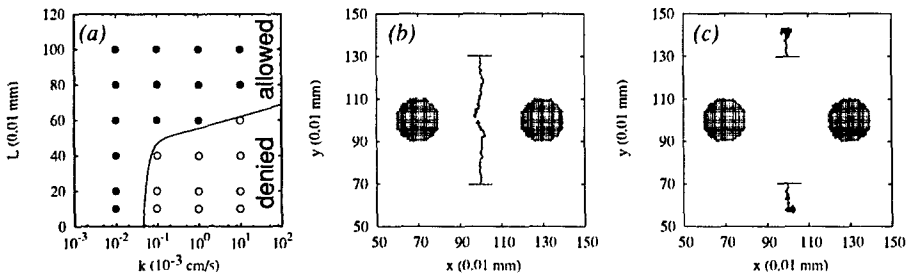

Figure 5. (a) "Phase-diagram" of successful passage of signaling, chemotactically responsive cells through a gap of size L defined by two circular obstacles with boundaries with reactivity k. Solid points denote the region in (L,k)-space for which passage is allowed, and open symbols those regions where passage is not allowed. In all cases, $\beta = 0.30$. (b) Example locomotion paths for a gap spacing of 0.4 mm and $k = 0$. Horizontal line segments denote the launch positions. (c) Same as (b), with $k = 1.0$.

obstacle boundary reactivity, the closer are the cells pushed toward the global boundary while moving toward one another. These results again demonstrate that chemotactically active mobile cells respond predictably to the presence of obstacles with surfaces that consume chemoattractant.

Dual walks around dual obstacles

We now turn to our simulations of two mobile chemotactically active cells separated by a gap defined by two circular obstacles (figure 2c). The two cells on either side of the gap secrete chemoattractant in pulses describing a random duty cycle which is known to result in successful chemotaxis in a homogeneous domain. Our objective was to determine how both the gap spacing L and the surface reactivity, k, both dictate whether one or both cells can enter or pass through the gap. In figure 5a, we report in phase-diagram format the results of our dual-walker simulations at various gap spacings L and obstacle boundary reactivities, k. Solid points represent those values of L and k for which one or both of the cells pass through the gap successfully, while the open symbols refer to those cases for which no successful passage through the gap is observed. We have considered gap spacings generally between 0.2 and 1.2 mm, much larger than an EC (~ 10 μm) or the minimal pore size through which ECs are known to pass (~ 60 μm). For low k, no hindrance to passage is observed for any gap size considered; an example of locomotion paths for $k = 0$ and $L =$ 0.4 mm is shown in figure 5b. However, at moderate to high reactivities, gap sizes of 0.2 - 0.5 mm prevent passage; an example of locomotion paths for for $k = 10^{-3}$ cm/s and $L =$ 0.4 mm is shown in figure 5c. One can see that the cells are simply forced away from the gap by the reactive obstacles. Because of the system's symmetry, cells are not able to acquire signal from one another by moving off the centerline, so cells are prevented from reaching one another, in contrast to the case with the single obstacle. This is somewhat

surprising: apparently, obstacle boundary reactivity in this particular gap geometry can raise by an order of magnitude the minimal gap size allowed for passage of a chemotactically active cell.

We undertook this study as a first attempt to understand how an imposed geometrical length scale (such as a pore size in a porous domain) together with chemoattractant transport with possible surface reactions influence chemotactic cell behavior. Clearly, both parameters are important, as demonstrated by figure 5a. It remains to be seen whether this understanding can be translated into the behavior of chemotactically active cells navigating through a fully random porous domain in three dimensions, which is our current object of study.

CONCLUSIONS

We have developed a simulation-based model of the locomotion of cells which both secrete and detect chemoattractant, coupled to transient concentration fields of this chemoattractant, for 2D heterogeneous domains with boundaries that consume (or produce) the chemoattractant. This model serves as a preliminary step toward developing a comprehensive model of chemically-stimulated tissue ingrowth in porous scaffolds, and is particularly suited to modeling angiogenesis. Clearly, chemotactic response is not the only phenomena governing tissue ingrowth; transport of nutrients and wastes, as well as, cell adhesion, spreading, proliferation must eventually be taken into account. We have simply sought to understand better the possible roles played by chemotactive response given that (a) cells use diffusing cytokines to signal one another, and these signals are a crucial element of tissue growth, and (b) in porous media, the chemical nature of the surfaces can be engineered. We have found that the presence of obstacles with reactive surfaces greatly influences the chemotactic response of crawling cells. Generally, reactive surfaces repel migratory cells which would normally respond by moving in the direction of increasing concentration. We have seen that moderate surface reactivities are sufficient to prevent successful transmission of chemical signals through gaps much wider than the minimum required for cell transit. These results, while applicable only in a generic sense, hint at possible mechanisms for guiding the directionality and speed of cell migration with fine detail, possibly offering guidance as to how to engineer chemically the internal pore surfaces of a porous scaffold to enhance the likelihood of successful tissue ingrowth.

ACKNOWLEDGMENTS

The authors gratefully acknowledge the National Science Foundation for financial support through grant BES-0331191.

References

[1] A. L. Sieminski and K. J. Gooch. *Biomaterials*, 21:2233–2241, 2000.

[2] B. D. Ratner. *J. Control. Release*, 78:211–218, 2002.

[3] A. A. Sharkawy, B. Klitzman, G. A. Truskey, and W. M. Reichert. *J. Biomed. Mater. Res.*, pages 586 597, 1998.

[4] T. D. Dziubla, M. C. Torjman, J. I. Joseph, M. Murphy-Tatum, and A. M. Lowman. *Biomaterials*, 22:2893–2899, 2001.

[5] W. Risau. *Nature*, 386:671, 1997.

[6] M. A. Golden, S. R. Hanson, T. R. Kirkman, P. A. Schneider, and A. W. Clowes. *J. Vasc. Surg.*, 11:838 844, 1990.

[7] K. R. Kidd, R. B. Nagle, and S. K. Williams. *J. Biomed. Mater. Res.*, 59:366–377, 2001.

[8] J. E. Sanders, S. G. Malcolm, S. D. Bale, Y.-N. Wang, and S. Lamont. *Microvasc. Res.*, 64:174 178, 2002.

[9] M. Gardner. *Scientific American*, pages 120–123, 223.

[10] K. Zygourakis, R. Bizios, and P. Markenscoff. *Biotechnol. Bioeng.*, 38:459–470, 1991.

[11] Y. Lee, S. Kouvroukoglou, L. V. McIntire, and K. Zygourakis. *Biophys. J.*, 69:1284–1298, 1995.

[12] S. M. Peirce, E. J. van Gieson, and T. C. Skalak. *FASEB J.*, 18(2), 2004.

[13] C. L. Stokes and D. A. Lauffenburger. *J. Theor. Biol.*, 3:377 403, 1991.

[14] S. Tong and F. Yuan. *Microvas. Res.*, 61:14 27, 2001.

[15] B. D. Sleeman and I. P. Wallace. *Math. Comput. Modelling*, 36:339 358, 2002.

[16] E. Jabbarzadeh and C. F. Abrams. Chemotaxis and random motility in time-varying concentration fields: A computational study. submitted to *J. Theo. Biol.*

[17] P. Gordon. *J. Soc. Ind. Appl. Math*, 13:667, 1965.

[18] A. R. Gourlay. *J. Inst. Math. Appl.*, 6:375–390, 1970.

[19] K. Francis and B. O. Palsson. *Proc. Nati. Acad. Sci. USA*, 94:12258–12262, 1997.

[20] S. H. Zigmond. *J. Cell Biol.*, 75:606 616, 1977.

[21] G. Serini, D. Ambrosi, E. Giraudo, A. Gamba, L. Preziosi, and F. Bussolino. *EMBO J.*, 22(8):1771–1779, 2003.